ICSV13 - Vienna
The Thirteenth International Congress on Sound and Vibration
Vienna, Austria, July 2-6, 2006

ROTOR DYNAMIC ANALYSIS OF A SYSTEM WITH A FLEXIBLE SHAFT AND JOURNAL BEARINGS

Dr. Ali T. Herfat

Emerson-Copeland Corporation, 1675 West Campbell Road, Sidney, OH 45365, USA, and
Adj Professor, University of Cincinnati, OH
Phone: (937) 493-2898, Fax: (937) 493-2366 USA, atherfat@copeland-corp.com

Abstract

Hydrodynamic interaction between a rotating shaft (journal) and its associated bearing is an indication of the load capability assessment of this system. Shaft deflection and roughness of the bearing surfaces are the significant causes in limiting the load capacities of journal bearings. The shaft deflection limits the load capacity of full journal bearings to magnitudes less than the value estimated by hydrodynamic theory. The higher the load on the shaft, the larger the journal misalignment resulted from shaft deformation, and the more obvious effect on lubrication performance of journal bearing. Structural dynamic analysis of machine or system presents the mode shapes, including the constraint modes and frequencies of the components as well as the natural frequencies and mode shapes of the complete machine or system. The flexible shaft mode shapes predict the possibilities of the edge loading or direct contact between journal-bearing and shaft. The objectives for this analysis presented in this paper are: 1) To estimate the stress generated on the bearing housing and transferred to machine casing or shell due to unbalance excitation on the rotor and/or bearing-housing misalignments during manufacturing. 2) The load capacity of the bearing with flexible shaft can be predicted to a rational order of magnitude. 3) The analysis results also show obvious changes at distribution and value of oil film pressure, oil film thickness and oil temperature of journal bearing due to journal misalignment.

INTRODUCTION

The dynamic behavior of a rotating machine is considerably affected by the characteristics of the flexibility of rotor and/or support of the machine. Rotor unbalance can also be caused by design, material, manufacturing and assembly. In reality this unbalance is an infinite number of unbalance vectors, distributed along the shaft axis of the rotor, of different magnitude and angular direction. The flexible rotor should not be deformed more than an acceptable magnitude defined in the design running speed range. The journal bearing edge loading is one of the most important reliability issues in the rotating machines. A resonant in a lightly damped structure can result in excessive vibration response. In such cases it may be more feasible to alter the natural frequency or damping of the structure rather than to balance to very low vibration levels as a result of unbalance issue. Using a flexible rotor model gives more accurate analytical results than the rigid rotor model.

The lubrication analysis is usually focused on tribological behavior without considering influences of other mechanical factors, so that the axis of the journal is usually supposed to be parallel to the center line of bearing. Shaft deformation caused by increasing load results in journal misalignment inside the bearing, thus lubrication state of the journal bearing will be influenced by the shaft deformation. Therefore, the shaft deformation should be considered in journal bearing and shaft design criteria as well as in the tribological analysis of journal bearing of machine.

The design optimization process should be involved in the rotordynamic analysis when there is structural complicity associated with the machine components.

DYNAMIC MODELING AND ANALYSIS OF A ROTOR SYSTEM WITH FLEXIBLE SHAFT

Dynamic Modeling using the Analytical Method

The planar rotor model is the simplest rotor model. This model considers only the motion of the rotor in the plane which is perpendicular to the rotating shaft. The geometric setup of the planar rotor model is shown in Figure 1.

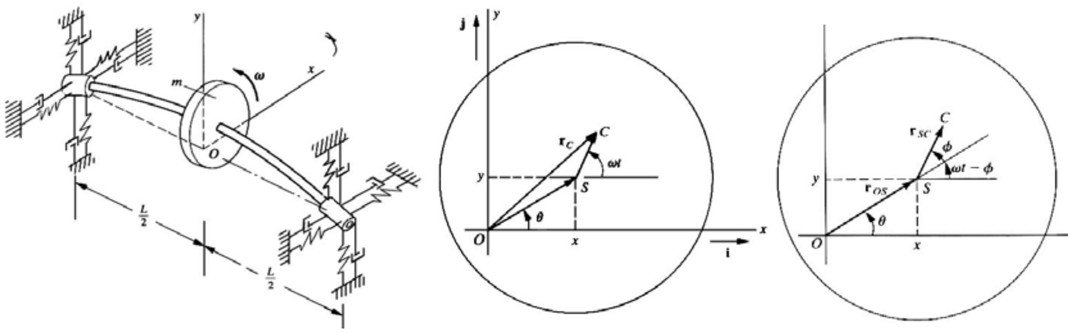

Figure 1. Geometric Setup of the Planar Rotor

Rotating Machine with Unbalanced Masses

The rotor system model represented in Figure *2a* consists of a main mass ($M - m$) and two eccentric masses $m/2$ rotating in opposite directions with the constant angular velocity ω. The reciprocating eccentric masses exert on the main mass two vertical forces F_x that add up and two horizontal forces F_y that cancel each other out, therefore it is only necessary to consider the vertical motion $x(t)$. By measuring the displacement $x(t)$ from the equilibrium position, the effect of the weight of the masses can be ignored in the equation of motion. The vertical displacement of the eccentric mass is $x(t) + l \sin \omega t$, so that the equations of motion in this direction for both m and *(M-m)* are given as

$$F_x = \frac{m}{2}\frac{d^2}{dt^2}\left[x(t) + l \sin \omega t\right] = \frac{m}{2}\left[\ddot{x}(t) - l\omega^2 \sin \omega t\right] \text{ and } -2F_x - c\dot{x}(t) - 2\frac{k}{2}x(t) = (M-m)\ddot{x}(t)$$

Substituting F_x from the Equation on left into the right one gives the equation of motion

$$M\ddot{x}(t) + c\dot{x}(t) + kx(t) = ml\omega^2 \sin \omega t = \mathrm{Im}(ml\omega^2 \sin \omega t) \tag{1}$$

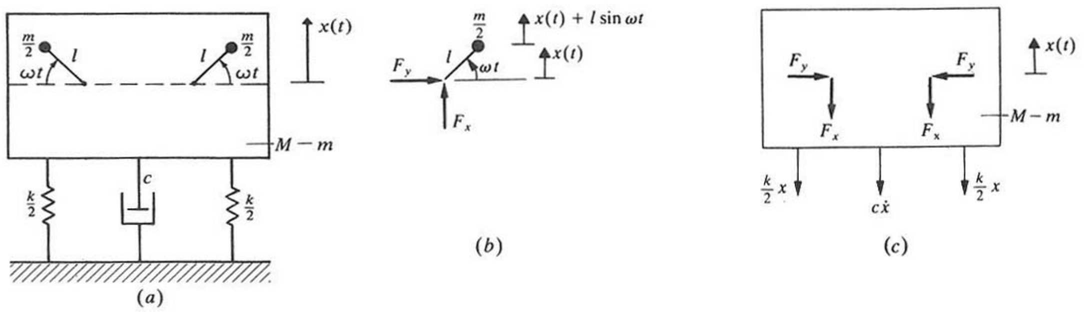

Figure 2. Rotor system with rotating unbalanced masses

The "*Im*" presents the imaginary expression. Hence, rotating eccentric masses exert a harmonic excitation on the system. The response is derived from Equation (1)

$$x(t) = \mathrm{Im}\left[\frac{m}{M} l \left(\frac{\omega}{\omega_n}\right)^2 \left|G(i\omega)\right| e^{i(\omega t - \phi)}\right] \tag{2}$$

in which the phase angle $|G(i\omega)|$ and ϕ are presented as

$$\left|G(i\omega)\right| = \frac{1}{\sqrt{(1-\omega/\omega_n)^2 + (2\xi\omega/\omega_n)^2}}, \quad \text{and} \quad \phi = \tan^{-1}\frac{2\zeta\omega/\omega_n}{1-(\omega/\omega_n)^2} \tag{3}$$

Writing the steady state response of Equation (1) in the form

$$x(t) = X \sin(\omega t - \phi) \tag{4}$$

Comparing Equations (2) and (4) gives

$$X = \frac{ml}{M}\left(\frac{\omega}{\omega_n}\right)^2 \left|G(i\omega)\right| \tag{5}$$

It is seen that for $\omega \to 0$, $(\omega/\omega_n)^2|G(i\omega)| \to 0$, and for $\omega \to \infty$ $(\omega/\omega_n)^2|G(i\omega)| \to 1$. Equation (3) shows that as $\omega \to \infty$ $\phi \to \pi$. Since the mass (M – m) undergoes the displacement $Im\ x$, whereas the mass m undergoes the displacement $Im\ (x + le^{i\omega t})$, it follows that for large driving frequencies ω the masses $(M - m)$ and m move in such a way that the mass center of the system tends to remain stationary. This is true regardless of the amount of damping.

Whirling of the Rotating Shafts

In the rotating machines, on occasions some of the shafts experience violent vibration. To explain this phenomenon, let us consider a rotating shaft carrying a single disk. If the disk has some eccentricity, then the rotation produces a centrifugal force causing the shaft to bend. The rotation of the plane containing the bent shaft about the bearings axis is known as *whirling.*

Figure 1 shows a shaft rotating with the constant angular velocity ω relative to the inertial axes x, y. The shaft carries a disk of total mass m at midspan and is supported elastically at both ends. Because the shaft has distributed mass, the system has an infinite number of degrees of freedom. However, if the mass of the shaft is small relative to the mass of the disk, then the motion of the system can be described approximately by the displacements x and y of the geometric center S of the disk. Although this implies a two-degree-of-freedom system, the x and y motions are independent, so that the solution can be carried out as for two systems with one degree of freedom each.

As a preliminary to the derivation of the equations of motion, we denote the origin of the inertial system x, y by O and the center of mass of the disk by C, where C is at a distance e from S, as shown in Figure 1. The equations of motion involve the acceleration a_c of the mass center C. To compute a_c, we first write the radius

$$r_c = (x + e\cos\omega t)i + (y + e\sin\omega t)j, \quad a_c = \left(\ddot{x} - e\omega^2\cos\omega t\right)i + \left(\ddot{y} - e\omega^2\sin\omega t\right)j \quad (6)$$

To derive the equations of motion, we assume that the only forces acting on the disk are restoring forces due to the elastic supports and the elasticity of the shaft and resisting forces due to viscous damping. The elastic effects are combined into equivalent spring constants k_x and k_y in the x and y directions, respectively. Moreover, we assume that c the coefficient of viscous damping is the same in both directions. Therefore, the equations of motion are written as

$$\begin{matrix} -k_x x - c\dot{x} = m\left(\ddot{x} - e\omega^2\cos\omega t\right) \\ -k_y y - c\dot{y} = m\left(\ddot{y} - e\omega^2\cos\omega t\right) \end{matrix} \quad or \quad \begin{matrix} \ddot{x} + 2\zeta_x\omega_{nx}\dot{x} + \omega_{nx}^2 x = e\omega^2\cos\omega t \\ \ddot{y} + 2\zeta_y\omega_{ny}\dot{y} + \omega_{ny}^2 y = e\omega^2\cos\omega t \end{matrix} \quad (7)$$

The steady-state solution of Equation (7) can be written as

$$x(t) = X(\omega)\cos(\omega t - \phi_x) \quad y(t) = Y(\omega)\sin(\omega t - \phi_y) \quad (8)$$

where the individual amplitudes in frequency domain are

$$X(\omega)=e\left(\frac{\omega}{\omega_{nx}}\right)^2 |G_x(i\omega)| \qquad Y(\omega)=e\left(\frac{\omega}{\omega_{ny}}\right)^2 |G_y(i\omega)| \tag{9}$$

and magnification factors and phase angles are defined as

$$|G_x(i\omega)|=\frac{1}{\left\{\left[1-(\omega/\omega_{nx})^2\right]^2+(2\zeta_y\omega/\omega_{nx})^2\right\}^{1/2}},\ |G_y(i\omega)|=\frac{1}{\left\{\left[1-(\omega/\omega_{ny})^2\right]^2+(2\zeta_y\omega/\omega_{ny})^2\right\}^{1/2}} \tag{10}$$

$$\phi_x=\tan^{-1}\frac{2\zeta_x\omega/\omega_{nx}}{1-(\omega/\omega_{nx})^2} \qquad \phi_y=\tan^{-1}\frac{2\zeta_y\omega/\omega_{ny}}{1-(\omega/\omega_{ny})^2} \tag{11}$$

Discussions: Case 1) the stiffness is the same in both directions, $k_x = k_y = k$. In this case, the two natural frequencies coincide and so do the viscous damping factors, or

$$\omega_{nx}=\omega_{ny}=\omega=\sqrt{\frac{k}{m}} \qquad \xi_x=\xi_y=\xi=\frac{c}{2m\omega_n},\ \text{and}\ X(\omega)=Y(\omega)=e\left(\frac{\omega}{\omega_n}\right)^2|G(i\omega)|$$

But, considering Figure 1 and Equation (8), gives

$$\tan\theta=\frac{y}{x}=\tan(\omega t-\phi),\ \ \theta=\omega t-\phi,\ \ \text{and}\ \dot{\theta}=\omega \tag{12}$$

Hence, in this case the shaft whirls with the same angular velocity as the rotation of the disk, so that the shaft and the disk rotate together as a rigid body. This case is known as *synchronous whirl.* It is easy to verify that in synchronous whirl the radial distance from O to S is constant, or

$$r_{os}=\sqrt{x^2+y^2}=e\left(\frac{\omega}{\omega_n}\right)^2|G(i\omega)|=const \tag{13}$$

so that point S describes a circle about point O and presented by Equation (13). From Figure 1, it can be interpreted that the phase angle ϕ as the angle between the radius vectors r_{os} and r_{sc}. It can be concluded that $\phi < \pi/2$ for $\omega < \omega_n$, $\phi = \pi/2$ for $\omega = \omega_n$, and $\phi > \pi/2$ for $\omega > \omega_n$.

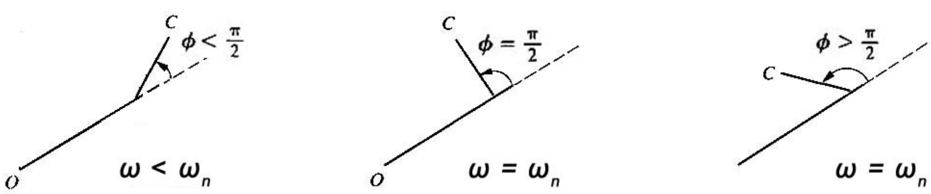

Figure 3. Synchronous whirl vs phase angles

The three configurations are shown in Figure 3. Concerning synchronous whirl, the magnification factor and the phase angle have the same expressions as in the case of the rotating unbalanced masses. This should come as no surprise as the two phenomena are entirely analogous.

Case 2) the two stiffnesses are different ($k_x \neq k_y$) and $c = 0$. In this case

$$x(t) = X(\omega)\cos \omega t \qquad y(t) = Y(\omega)\sin \omega t \tag{14}$$

$$X(\omega) = \frac{e(\omega/\omega_{nx})^2}{1-(\omega/\omega_{nx})^2} \qquad Y(\omega) = \frac{e(\omega/\omega_{ny})^2}{1-(\omega/\omega_{ny})^2}$$

Dividing the first of Equation. (14) by $X(\omega)$ and the second one by $Y(\omega)$, squaring and adding the results, yields

$$\frac{x^2}{X^2} + \frac{y^2}{Y^2} = 1 \tag{15}$$

Hence, as the shaft whirls, point S describes an ellipse with point O as its geometric center, and Consider Equation (14) to understand more about the motion, and write

$$\tan\theta = \frac{y}{x} = \frac{Y}{X}\tan\omega t \quad \text{and} \quad \dot{\theta} = \frac{XY}{X^2\cos^2\omega t + Y^2\sin^2\omega t}\,\omega \tag{16}$$

the sign of $\dot{\theta}$ depends on the sign of $X\,Y$. By convention, the sign of ω is assumed as positive, i.e., the disk rotates in the counter-clockwise sense. Thus, the following cases can be understood:

a) $\omega < \omega_{nx}$ *and* $\omega < \omega_{ny}$. In this case $X\,Y > 0$, so that point S moves on the ellipse in the same sense as the rotation ω.
b) $\omega_{nx} < \omega < \omega_{ny}$ or $\omega_{ny} < \omega < \omega_{nx}$. In either of these two cases $X\,Y < 0$, so that S moves in the opposite sense from ω.
c) $\omega > \omega_{nx}$ and $\omega > \omega_{ny}$. In this case $X\,Y > 0$, so that S moves in the ω direction.

It is concluded that the possibility of resonance can be existed for the undamped case. There are two frequencies for which resonance is possible, $\omega = \omega_{nx}$ and $\omega = \omega_{ny}$. Clearly, in the case of resonance, Equation (14) are no longer valid. The two frequencies $\omega = \omega_{nx}$ and $\omega = \omega_{nx}$ are called *critical frequencies.*

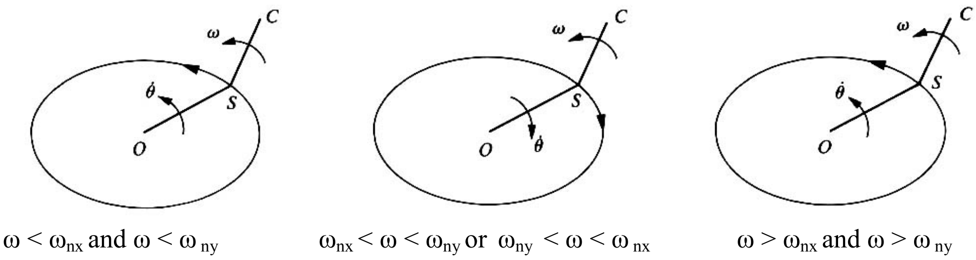

Figure 4. The three cases, asynchronous whirl

Machine Elements Structural Analysis

Usually rotors are modeled using beam theory, with either the Euler-Bernoulli or the Timoshenko approach. Numerical solutions based on the transfer matrix method are also a common approach. In the study of the torsional behavior of shafts the structural parts are mainly modeled as beams. If the beams which model the rotor are straight, their axes are all aligned with the spin axis and if the centre of gravity and the shear centre of all the cross sections lay on the spin axis, then the axial, flexural and torsional behaviors are uncoupled. The presence of a small static or couple unbalance does not modify substantially this feature. The assumptions of linearity, small unbalance and small displacements allow obtaining a linear equation of motion; however, even in the case of the discretized model of a linear rotor which is axially symmetrical about its spin axis and rotates at a constant spin speed ω. If both stator and rotor are isotropic with respect to the rotation axis, the best choice for the generalized coordinates to study the flexural behavior is using the complex coordinates. The linearized equation of motion that are linearized in the neighborhood of an operating point constant rotating speed is of the type

$$[M]\left\{\ddot{q}\right\}+\left(C+iG_{sk}\right)\left\{\dot{q}\right\}+\left(K+iK_{sk}\right)\{q\}=f(t)$$

where q is a vector containing the generalized complex coordinates, referred to an inertial frame, M and C *are* the symmetric rotor system mass damping matrixes, G_{sk} is the skew-symmetric gyroscopic matrix (it is usually linearly dependent on the pin speed ω, K is the symmetric rotor system stiffness matrix, K_{sk} is the skew-symmetric circulatory matrix, usually proportional to ω and f is a time-dependant vector in which all forcing functions are included. One of these forcing functions is usually due to the residual unbalance which, although small, cannot be neglected. Unbalance forces are harmonic functions of time, with amplitude proportional to ω^2 and frequency equal to ω. When ω tends to zero, the skew-symmetric terms vanish and the rotor reduces to a structure.

The finite element method has ability of complicated geometries modeling in a simple way. The Finite element codes are flexible and powerful enough, if they have some of the numerical features (such as gyroscopic effect, rotating damping and centrifugal stiffening) that are used for rotordynamics.

The transfer matrix method is mostly used in the rotor dynamic analysis. The advantage of the transfer matrix method to finite element technique is that it does not require the storage and manipulation of large system arrays. The transfer matrix method begins with the boundary conditions at one side of the system and successively proceeds along the structure to the other side including all the components. The solution should satisfy all the boundary conditions at all boundary points. The disadvantage of this method is that it is difficult to extend to time domain and nonlinear analysis. Therefore, it is difficult to use this method for active balancing controller design analysis. The resonant vibration amplitude is smaller than the corresponding amplitude if the spin speed is held constant at the critical speed.

Rotating Machine, Experimental Dynamic Analysis

The experimental procedure is divided in three parts: 1) The Campbell diagram that gives the development of the eigenvalues of the rotor as a function of the rotation speed is established. 2) Unbalance response of the rotor is undertaken as a function of rotational speed. Typically the natural frequencies change with speed because of gyroscopic effects and bearing characteristics. 3) The influence of flexible support.

For the isotropic supports and the symmetric rotor, an excitation (with a sweep sine approach) is acted on the bearing housing in order to evaluate the frequency response function of several rotating speeds. Whirl modes appear due to the asynchronous excitation given by the electromagnetic shaker. The Campbell diagram of the rotor that represents the natural frequencies as a function of rotational speed is illustrated in Figure 5. Note that when the first forward and backward modes start at different values indicating asymmetric properties for the rotor.

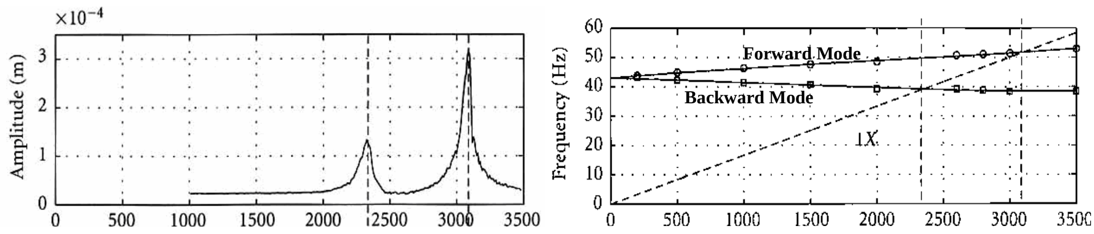

(a) Rotating Speed (rpm) (b) Rotating Speed (rpm)

Figure 5: Unbalanced response: (a) it shows two responses: The first response at 2340 rpm (first backward critical speed) and the second response at 3080 rpm (the first forward critical speed). (b) the Campbell diagram of the rotor (evolutions of the natural frequencies as a function of the rotational speed).

Tribology and Lubrication criteria, Experimental Measurements

When a rotating machine rotates, the centrifugal force produced by eccentric weight results in shaft deformation. The magnitude of journal misalignment corresponding to the magnitude of shaft deformation can be adjusted by regulating the magnitude of centrifugal force acting on the shaft. Assume the effect of weight gravity on shaft deformation is negligible comparing with the centrifugal force, in order of magnitude. The testing system rig is shown in Figure 6 consists of sensors, data acquisition and analyzing system. The sensors are installed separately on section A-A and section B-B near the two ends and symmetric to the central section of the measured bearing and they are used to measure oil film pressure, oil film thickness, and oil film temperature near the surface of the bearing at any instant. The rotating angle and speed sensor measure the shaft speed and orientation of the load acting on the shaft along the circumferential direction.

The shaft speed has been increased up to 3500 r/min. The results of these experiments are shown in Figure 6. When shaft load (at the center of shaft) increases, the maximum film pressure and average film temperature generally increase, and the minimum film thickness decreases. There is an indication of scratches at the edge of the bearing near section A-A. When the angle of journal misalignment is large at the time so that the minimum film thickness on section A-A is very small. Radial clearance has a large effect on average film temperature, the smaller the radial clearance, the higher the average film temperature.

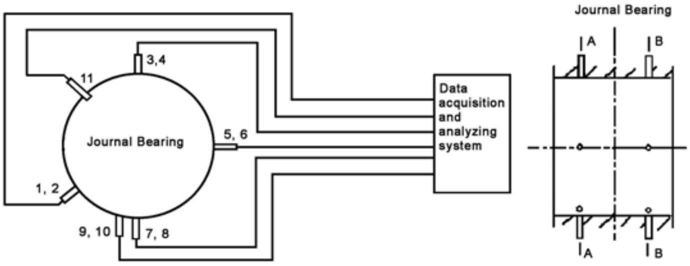

Figure 6: Sensors at A & B sections of journal bearing: I) Pressure transducers: 1, 2, 3, 4. II) Whirl type sensors (Eddy current): 4 5, 6, 7, 8. III) Thermocouples: 9, 10. IV) Speedometer sensor: 11.

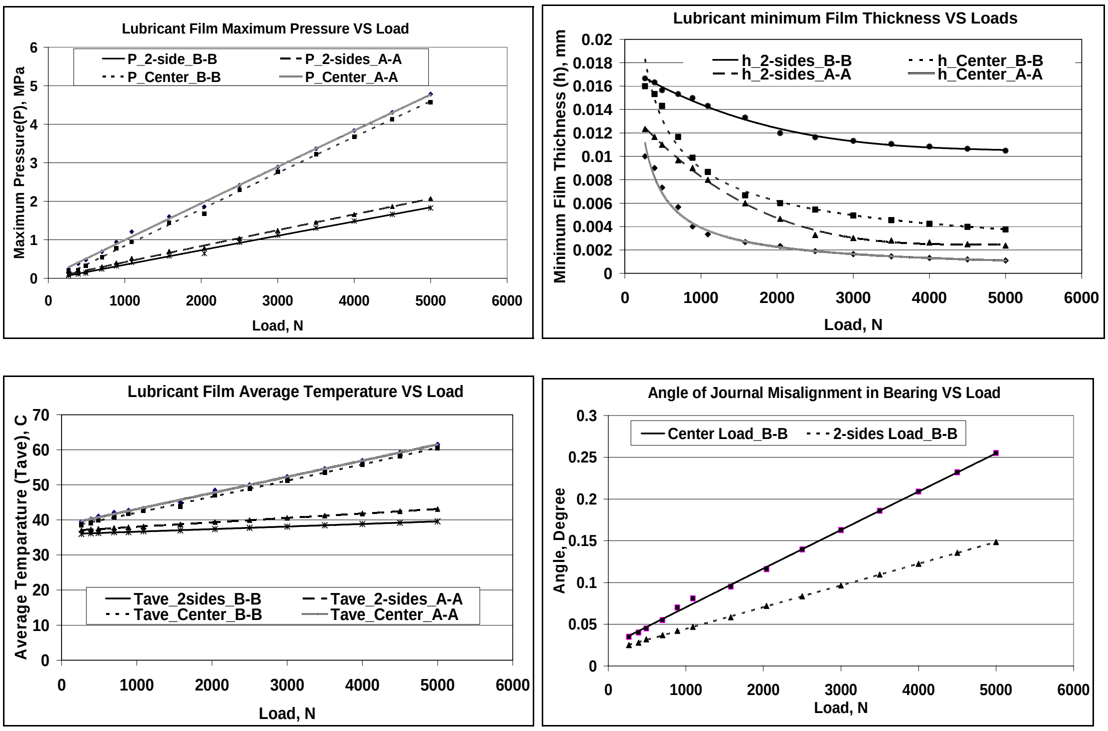

Figure 7: The experimental results

It should be noted that the shaft deformation with shaft load acting on the two sides of the shaft is smaller than that with the same load acting on the center of the shaft if other conditions are the same.

The clearance of a bearing c of 0.045, bearing length L of 40 mm, and bearing diameter D of 30 mm with shaft load acting on the center and or at the two sides of the shaft have been chosen in this experimental study. The experimental results are shown in Figures 7

SUMMERY AND CONCLUSIONS

An in depth knowledge of the dynamic behavior of rotating machines are required when high rotational speeds, lighter machines (higher performance), and working at higher stress levels are involved in the design of rotating components. The following concerns should be considered in the rotor dynamic analysis:

1. Shaft deformation under load will cause journal misalignment in shaft-journal bearing systems.
2. Oil film pressure, oil film thickness, and oil temperature at corresponding positions of two sections, symmetric with respect to the central section of the bearing, are different when there journal misalignment occurs due to the shaft deformation. Changes of oil film pressure, oil film thickness and oil temperature of the bearing compared with a well-aligned bearing are seen clearly.
3. The differences of the values of the maximum film pressure, the minimum film thickness, and average film temperature at the two end sections symmetric about the central section of the bearing increase with shaft load, and the angle of journal misalignment result from increased shaft deformation.
4. The smaller the ratio of radial clearance c to length L of a bearing, the more obvious the effect of journal misalignment becomes dominantly from shaft deformation, and affecting the values and distributions of oil film pressure, oil film thickness and oil film temperature in a journal bearing.
5. The effect of journal misalignment resulting from shaft deformation should be considered in journal bearing design, especially for cases of critical mechanical equipments.

REFERENCES

1. Shigley & Mischke. *Standard Handbook of Mechanical Design*. (McGraw-Hill 1986)
2. J. S. Alford. *Protecting Turbomachinery from Self-excited RotorWhirl*. (ASME J. Eng. Power, 87,333, 1965)
3. W. Shapiro & Colsher. *Dynamic characteristics of fluid-film bearings*. (Proc. 6th Turbomachinery Symp., Texas A&M University, 39-54, 1977)
4. A. A. Raimondi. *A Numerical Solution for the Gas Lubricated Full Journal Bearing of Finite Length*. (*ASLE Transactions, vol.* 4, 1961, pp. 131-155. 28-12 E. R. Wu, "Gas-Lubricated Porous Bearings of Finite Length-Self-Acting Journal Bearings," *ASME Journal of Lubrication Technology, vol. 101, July* 1979, pp. 338-348).
5. M.A. Prohl, *A General Method for Calculating Critical Speeds of Flexible Rotors,* ASME Journal of Applied Mechanics 67, A142-A148, 1945.
6. G. Genta, A. Tonoli, *A Harmonic Finite Element for the Analysis of Flexural, Torsional and Axial Rotordynamic Behaviour of Discs*, Journal of Sound and Vibration, 196(1), 1996, pp. 19-43.
7. L. Meirovith, *Elements of Vibration Analysis,* (McGraw-Hill 1986)